

Coupled Air, Sea, and Land Interactions of the South American Monsoon

VASUBANDHU MISRA

Department of Meteorology, and Center for Ocean–Atmospheric Prediction Studies, The Florida State University, Tallahassee, Florida

(Manuscript received 25 February 2008, in final form 25 May 2008)

ABSTRACT

The dominant interannual variation of the austral summer South American monsoon season (SAM) is associated with El Niño–Southern Oscillation (ENSO). Although this teleconnection provides a basis for the seasonal predictability of SAM, it is shown that the conventional tier-2 modeling approach of prescribing observed sea surface temperature (SST) is inappropriate to capture this teleconnection. Furthermore, such a forced atmospheric general circulation model (AGCM) simulation leads to degradation of the SAM precipitation variability.

However, when the same AGCM is coupled to an ocean general circulation model to allow for coupled air–sea interactions, then this ENSO–SAM teleconnection is reasonably well simulated. This is attributed to the role of air–sea coupling in modulating the large-scale east–west circulation, especially associated with Niño-3 SST anomalies. It is also shown that the land–atmosphere feedback in the SAM domain as a result of the inclusion of air–sea coupling is more robust. As a consequence of this stronger land–atmosphere feedback the decorrelation time of the daily rainfall in the SAM region is prolonged to match more closely with the observed behavior.

A subtle difference in the austral summer seasonal precipitation anomalies between that over the Amazon River basin (ARB) and the SAM core region is also drawn from this study in reference to the influence of the air–sea interaction. It is shown that the dominant interannual precipitation variability over the ARB is simulated both by the uncoupled and coupled (to OGCM) AGCM in contrast to that over the SAM core region in southeastern Brazil.

1. Introduction

The basis for seasonal prediction of the tropical climate stems from the seminal works of Charney and Shukla (1981). Simply stated, it suggests that the slowly varying surface boundary conditions influence the atmospheric anomalies to a large part and, therefore, provide a scope for predictability beyond the short time scale of weather phenomenon. This gave impetus to a vast number of studies that adopted the tier-2 approach for seasonal and multidecadal integrations of the atmospheric general circulation model (AGCM) that used prescribed sea surface temperature (SST) as the surface boundary forcing (Sperber et al. 2001; Shukla et al. 2000; Gates et al. 1999; Gates 1992). These studies met with reasonable success in simulating some of the large tropical and subtropical seasonal anomalies associated

with the El Niño–Southern Oscillation (ENSO). However, there was a growing concern that some regions of the tropics were showing consistently poor results with this tier-2 approach (Wang et al. 2004; Gadgil and Sajani 1998). Furthermore, with growing demands for a credible prediction of seasonal and longer-term anomalies (Barnston et al. 2005, and references therein), the tier-2 approach of prescribing observed SST was found to be inappropriate. However, these AGCM seasonal and longer-term integrations were more commonly used to diagnose “potential predictability” (Shukla et al. 2000).

This demand for real-time forecasts however led to using AGCMs for seasonal predictions forced with a SST that is forecasted independently of the AGCM (Bengtsson et al. 1993). This approach continues to be used in operational prediction even now (Barnston et al. 2005; Goddard and Mason 2002). However, the conventional notion of atmospheric anomalies being a slave of (forced by) surface boundary anomalies especially over certain regions of the tropics has been challenged in some recent studies (Wu et al. 2006; Wang et

Corresponding author address: Vasubandhu Misra, Department of Meteorology, The Florida State University, 404 Love Building, Tallahassee, FL 32306.
E-mail: vmisra@fsu.edu

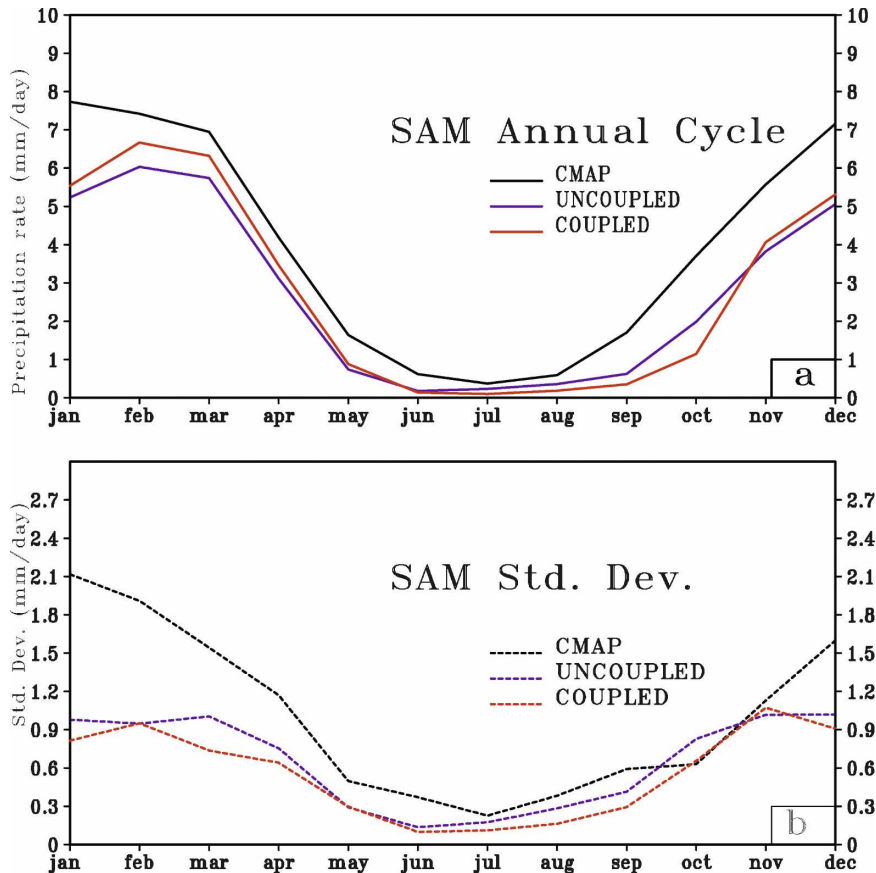


FIG. 1. The (a) climatological annual cycle and (b) standard deviation of monthly mean anomalies of precipitation averaged over SAM.

al. 2005; Kumar et al. 2005). The local rainfall–SST and heat flux–SST relationships in such forced AGCM integrations are found to be consistently erroneous in some regions of the tropics such as that over the tropical western Pacific Ocean. Wang et al. (2005) and Wu et al. (2006) have demonstrated that this error is directly related to the lack of air–sea coupling in the tier-2 approach.

In a similar vein, in this study it is demonstrated that such a coupled modeling framework, which incorporates the air–sea coupling, is essential to reproduce the observed interannual variations of the South American monsoon (SAM). This study is unique in its finding of the importance of air–sea interactions for the interannual variations of SAM. SAM has several common features that can be identified with a monsoon system (Vera et al. 2006; Grimm et al. 2005; Zhou and Lau 1998; Kousky 1985). The SAM core region is located in Brazil (5°S–20°S, 40°–60°W) (hereafter SAM; Vera et al. 2006). It is part of the many distinct regions of copious rainfall over the South American continent. The

northwest corner of this core region is a part of the Amazon River basin (ARB). This SAM region also includes the land component of the South Atlantic convergence zone (SACZ) to the south and southeast and the Nordeste region to the northeast. The SAM region has a distinct annual cycle (Fig. 1a; Vera et al. 2006) and interannual variability (Fig. 1b; Grimm et al. 2000; 2003) that is not far different from that over the neighboring Amazon River basin (5°N–15°S, 70°–50°W), as shown in Figs. 2a and 2b. It should be noted that the observed precipitation used in Figs. 1 and 2 is from the monthly mean dataset of the Climate Prediction Center (CPC) Merged Analysis Precipitation (CMAP) (Xie and Arkin 1996) from 1979 to 2005. However, there are subtle but important differences between the two regions, namely:

- 1) The annual cycle is more robust in the SAM region. In the season of December–February (DJF) the climatological seasonal mean precipitation over SAM is well above 7 mm day⁻¹, while in June–August

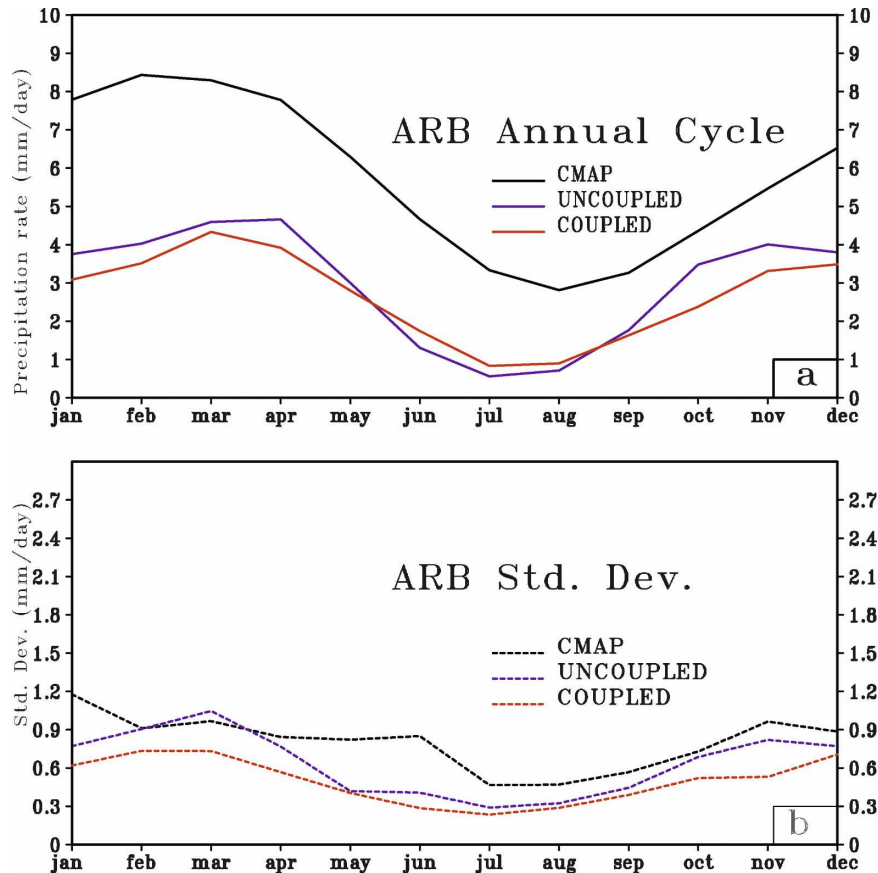


FIG. 2. As in Fig. 1 but over ARB.

(JJA) it is well below 1 mm day^{-1} . In contrast, over the ARB region DJF season receives around 8 mm day^{-1} compared to 4 mm day^{-1} in JJA.

- 2) Likewise, the annual cycle of the standard deviation of monthly mean precipitation has a stronger seasonal cycle over the SAM region compared to that over the ARB region. In addition to these differences, Liebmann et al. (1999) also point to differences in the subseasonal features of these two regions. Furthermore, seasonal predictability over the SAM region is a challenge for climate prediction. It includes parts of the Nordeste region, which is well known for high seasonal predictability (Folland et al. 2001; Misra 2004, 2006). However, the SAM region also includes parts of the SACZ, which is well known to have low seasonal predictability (Nobre et al. 2006; Misra 2004) owing to the strong influence of subseasonal variations and midlatitude intrusions of frontal systems (Kousky 1985; Garreaud and Wallace 1998; Garreaud 2000; Seluchi and Marengo 2000). In this study we shall be focusing on the rainy (DJF) season of the SAM and the ARB regions.

In the following section a brief description of the model is provided. This is followed by an explanation of the conducted experiments in section 3. In section 4 results are discussed followed by concluding remarks in section 5.

2. Model description

a. AGCM

The Center for Ocean–Land–Atmosphere Studies (COLA) coupled climate model (Misra et al. 2007) is used in this study. It comprises the AGCM version 3.2 at a spectral resolution of T62 with 28 terrain-following sigma ($=p/p_s$) levels, identical to the National Centers for Environmental Prediction–National Center for Atmospheric Research (NCEP–NCAR) reanalysis model (Kalnay et al. 1996). The dynamical core follows from the Eulerian core of the Community Climate Model version 3 (Kiehl et al. 1998) wherein the dependent variables are spectrally treated except for moisture, which is advected by a semi-Lagrangian scheme. The relaxed Arakawa–Schubert scheme [Moorthi and

Suarez (1992) and modified as in Bacmeister et al. (2000)] is used for deep convective parameterization. The longwave and shortwave radiation scheme is identical to that in the Community Climate System Model version 3.0 (Collins et al. 2006). The cloud optical properties follow from Kiehl et al. (1998). The planetary boundary layer is a nonlocal scheme (Hong and Pan 1996) and the shallow convection uses the formulation in Tiedtke (1984). The land surface scheme uses the Simplified Simple Biosphere (SSiB) scheme (Xue et al. 1991, 1996; Dirmeyer and Zeng 1999).

b. OGCM

This COLA AGCM is coupled to the Modular Ocean Model version 3.0 (MOM3) (Pacanowski and Griffies 1998). MOM3 covers the global oceans between 74°S and 65°N with realistic bottom topography. However, ocean depths less than 100 m are set to 100 m and the maximum depth is 6000 m. It has a uniform zonal resolution of 1.5° while the meridional resolution is 0.5° between 10°S and 10°N gradually increasing to 1.5° at 30°N and 30°S and fixed at 1.5° in the extratropics. The vertical mixing is the nonlocal K-profile parameterization of Large et al. (1994). The momentum mixing uses the space–time–dependent scheme of Smagorinsky (1963), tracer mixing follows Redi (1982), and the Gent and McWilliams (1990) quasi-adiabatic stirring is used.

3. Design of experiments

The coupled model results presented here are from the last 50 years of a 100-yr integration restarted from a previous coupled model integration (Misra and Marx 2007). The coupled mean state of the model is therefore well spun up. Here, we shall be analyzing the results from the last 50 years of this model integration. This experiment is hereafter referred to as COUPLED.

Similarly, the AGCM identical to that used in the COUPLED experiment is integrated for 100 years from 1901 to 2000 with the observed optimally interpolated SST version 2 (OISST2) following Reynolds et al. (2002). The atmospheric and land initial conditions are obtained from restart files of a previous coupled integration from the same model. The results are analyzed from the last 50 years of this integration. This experiment hereafter is called UNCOUPLED.

4. Results

a. Mean annual cycle of precipitation

In Figs. 1a and 2a, the climatological annual cycle of precipitation over the SAM and ARB regions are shown. As discussed earlier, the observed annual cycle

is much stronger in the SAM region compared to ARB. It should be noted that SAM onset has its precursors from early October when rain in excess of 4 mm day⁻¹ progresses from the northwest corner of the ARB region toward southeastern Brazil during the peak of the boreal winter season (Marengo et al. 2001; Kousky 1988). These features are reasonably well simulated by both COUPLED and UNCOUPLED experiments. Similarly, the annual cycle of the standard deviation of the monthly mean anomalies in the two experiments over the two regions compare well with observations (Figs. 1b and 2b). However, both model experiments underestimate the annual cycle and its standard deviation in SAM and ARB regions relative to the observations. This is primarily a result of the spurious alternating dry and wet bands of precipitation on the lee side of the Andes as a result of the Gibbs phenomenon from the spectral transformation of steep orography (Misra and Marx 2008).

b. Interannual variability

The interannual variability of the SAM has received considerable attention (Paegle and Mo 2002; Grimm et al. 2000, 2003; Grimm 2004; Nobre et al. 2006; Vera et al. 2006). These studies indicate that the leading mode of the interannual variations of precipitation over South America is found to be related to ENSO. During warm (cold) ENSO events, dry (wet) conditions prevail over northern South America and wet (dry) conditions over the subtropical plains.

The contemporaneous regression of the observed Hadley Center Global Sea Ice and Sea Surface Temperature (HadADISST) (Rayner et al. 2002) on the SAM area-averaged precipitation for DJF is shown from observations (CMAP) and the UNCOUPLED experiment in Figs. 3a and 3b, respectively. These are linear regressions, which obviously does not capture any existing nonlinear relationships. Unlike the observations, the mean DJF precipitation anomaly in the UNCOUPLED experiment is disconnected with the Niño-3 SST variability. However, the COUPLED experiment shown in Fig. 3c is able to recover this teleconnection pattern between SAM and the Niño-3 region. There are, however, some apparent differences between Figs. 3a and 3c, such as the response in SST is more westward in the COUPLED experiment. Additionally, the regression over the South Atlantic is weak in the COUPLED run compared to observations. These biases in the interannual variation of SAM precipitation are, in fact, a reflection of the ENSO bias in the COUPLED model. This is illustrated in Fig. 4, which shows the regression of the global tropical SST anomalies on the Niño-3 SST index. It is clearly seen in

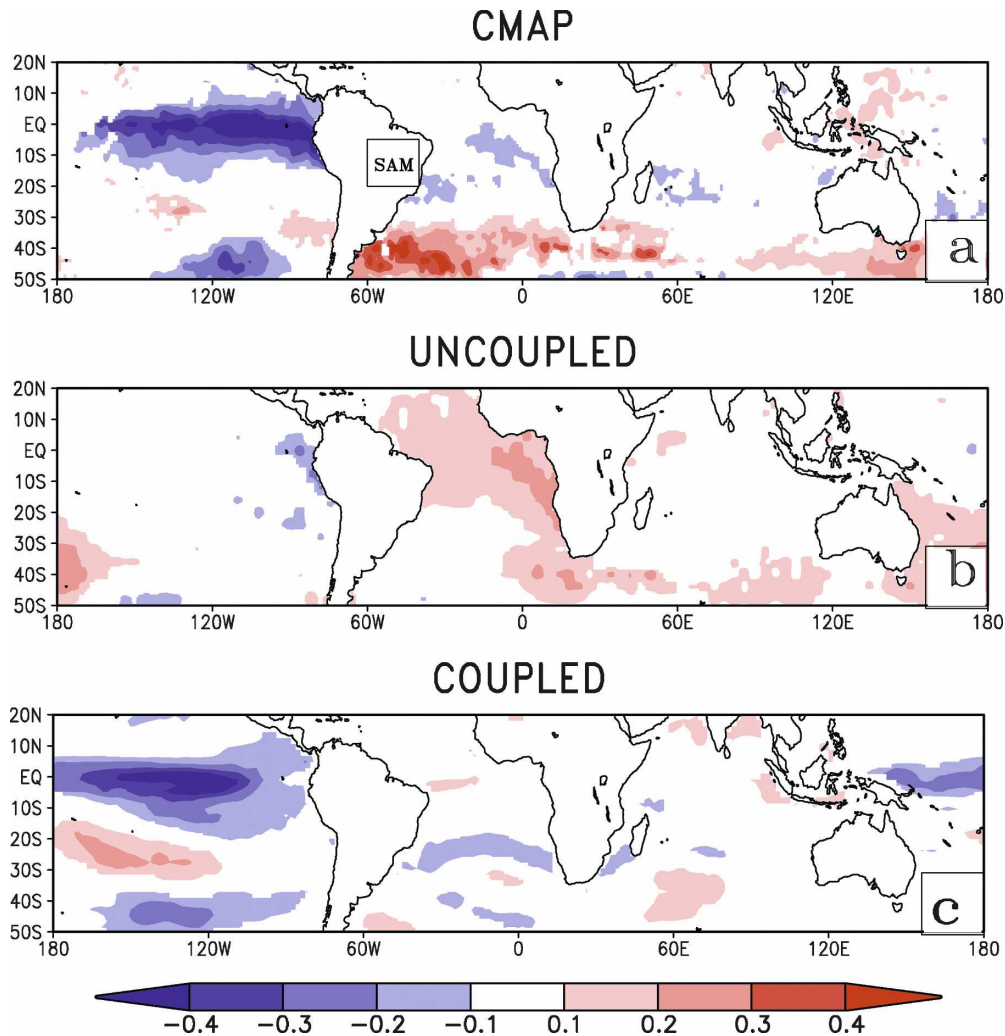


FIG. 3. Regression of the mean DJF SST on precipitation averaged over the SAM domain from (a) CMAP (the SAM is outlined), and (b) UNCOUPLED and (c) COUPLED integrations. The SST in (a) and (b) is from HADISST, while in (c) it is from the COUPLED integration. Only significant values at the 90% confidence interval according to a t test are plotted. Units: $^{\circ}\text{C}$.

this figure that, relative to observations (Fig. 4a), the COUPLED model has the SST anomalies extending farther westward beyond the date line. The subtropical SST anomalies both in the South Pacific and in the South Atlantic Oceans are weaker than in observations. The UNCOUPLED run (Fig. 3a) exhibits a teleconnection pattern of the SAM seasonal precipitation with equatorial and northern tropical Atlantic Ocean that is unsubstantiated from observations. Obviously the difference in the SAM precipitation teleconnection patterns with the global SST in the two model integrations can simply be attributed to the role of the air–sea coupling.

In contrast to the SAM region, the mean DJF precipitation anomaly over the ARB is rather insensitive

to the air–sea coupling. This is illustrated in Figs. 5a–c, which show a similar regression of the contemporaneous global mean DJF SST on precipitation area averaged over the ARB region from observations, UNCOUPLED, and COUPLED experiments, respectively. Significant response of ARB precipitation to anomalies of SST in the eastern equatorial Pacific is seen in both the UNCOUPLED and COUPLED experiments, consistent with the observations. There is a significant broad response over the north and eastern Atlantic Ocean in the UNCOUPLED run that is unsupported by observations. In fact, this pattern of erroneous Atlantic SST variability is also seen in Fig. 3b with the SAM precipitation. There are three plausible explanations for the differences over the SAM region

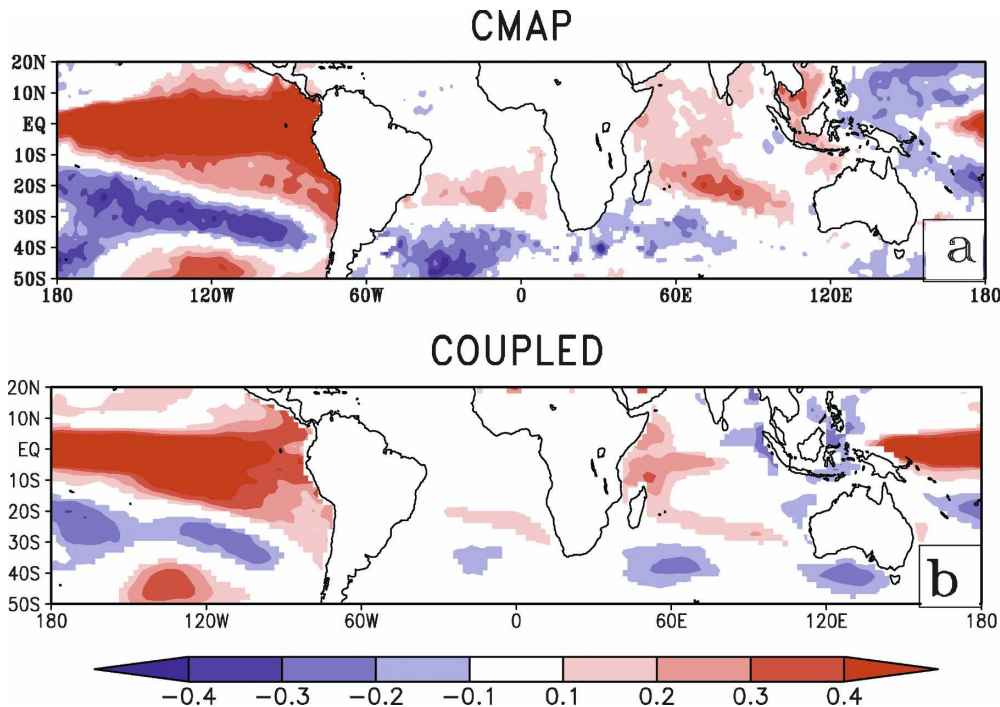


FIG. 4. Regression of the global tropical SST on the Niño-3 SST index. Only significant values at the 90% confidence interval according to a t test are plotted. Units: $^{\circ}\text{C}$.

between the COUPLED and UNCOUPLED simulations. They are discussed below.

c. Large-scale circulation

The large-scale circulation is modulated as a result of the inclusion (exclusion) of air–sea coupling in the COUPLED (UNCOUPLED) simulation. The climatological mean DJF velocity potential and divergent wind vectors at 200 hPa from the two model runs and the NCEP–NCAR reanalysis are shown in Fig. 6.

The climatological mean DJF velocity potential and divergent wind vectors at 200 hPa from the two model runs and NCEP–NCAR reanalysis are shown in Fig. 6. There are some significant differences in the mean upper-level circulation between the two models. In the UNCOUPLED model the ascending branch of the east–west Walker circulation described by the large negative values of the velocity potential is centered over the warm pool region of the western Pacific Ocean, which extends eastward toward the date line and, weakly, westward toward the equatorial Indian Ocean. The COUPLED integration displays the ascending branch of the Walker circulation that extends from the warm pool region of the western Pacific westward through the equatorial Indian Ocean and very weakly eastward toward the date line. The NCEP–NCAR reanalysis shows its main ascent over the warm

pool region of the western Pacific with insignificant ascent over the western equatorial Indian Ocean. Correspondingly, the descending branch of the Walker circulation also shows differences between the two integrations. The large-scale descent of climatological Walker circulation is stronger in the COUPLED run (but closer to the NCEP–NCAR reanalysis) compared to the UNCOUPLED integration over the Sahara, the northern Atlantic, and over the eastern Pacific Ocean. It is however important to note that Kinter et al. (2004) point to a model bias in the large-scale upper-level divergent circulations in the NCEP–NCAR reanalyses.

The anomalous large-scale upper-level (200 hPa) circulation obtained from regressing the mean DJF global velocity potential on the contemporaneous Niño-3 SST also shows significant differences between the UNCOUPLED and COUPLED integrations. This is illustrated in Fig. 7. The anomalous large-scale descent over the ARB (associated with a warm ENSO event) is stronger in the UNCOUPLED (Fig. 7a) than in the COUPLED (Fig. 7b) integration. In fact, in comparison with the NCEP–NCAR reanalysis (Fig. 7c), the large-scale anomalous divergent circulation in the COUPLED integration is relatively more verifiable than the UNCOUPLED integration. However, the anomalous descent over the Indo-Pacific region in the NCEP–NCAR reanalysis (during a warm ENSO

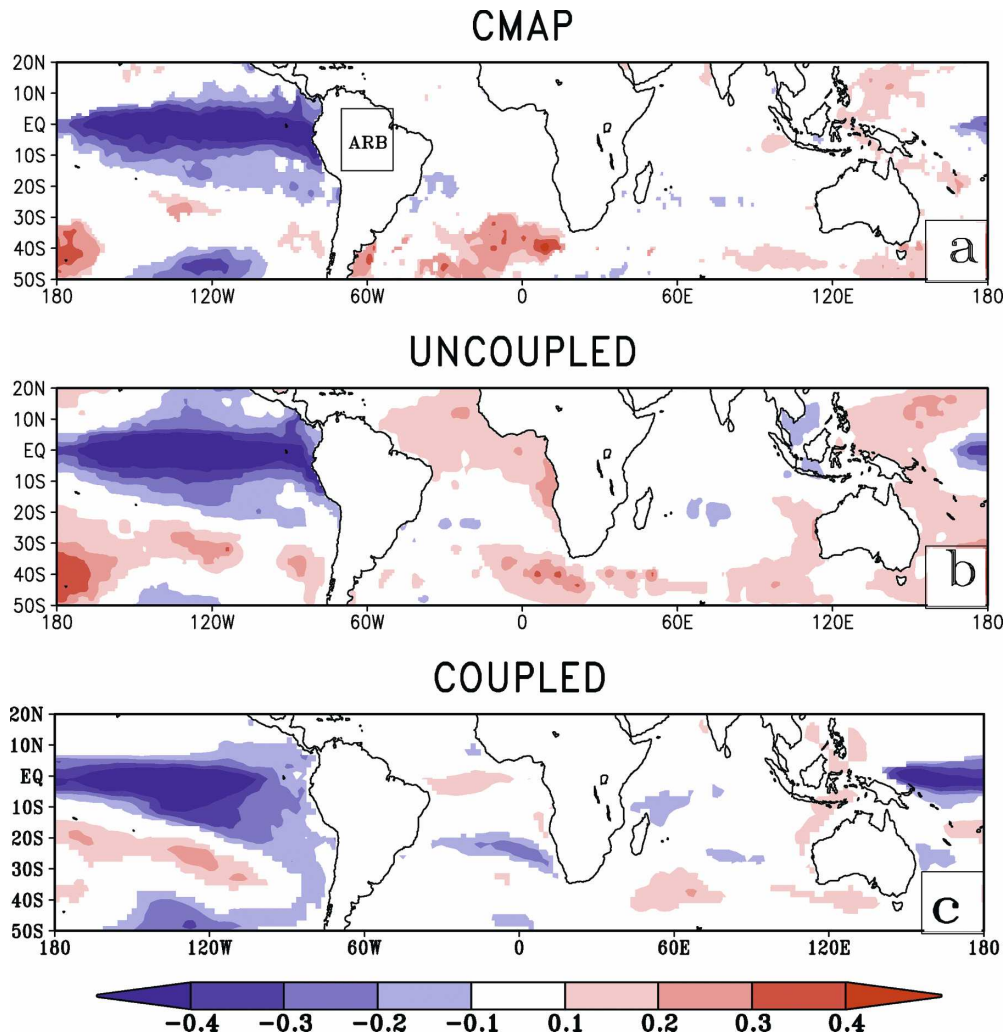


FIG. 5. As in Fig. 1 but with precipitation area averaged over the Amazon River basin, outlined in Fig. 2a.

event) is incorrectly simulated in the COUPLED and UNCOUPLED simulations. This is largely because the precipitation over the warm tropical Indian Ocean is erroneously large.

A similar regression of the mean DJF global streamfunction at 850 hPa on the contemporaneous Niño-3 SST is shown in Fig. 8. It should be mentioned that Newman et al. (2000) indicate that the rotational circulation is fairly well represented in the NCEP-NCAR reanalysis. In Figs. 8a and 8b both the UNCOUPLED and COUPLED simulations display apparent differences from the NCEP-NCAR reanalysis. In a typical warm ENSO year the tropical Pacific becomes warmer, pushing the midlatitude jets farther poleward, resulting in a weakening of the subtropical highs. This feature is more apparent in the Pacific in both integrations and in the NCEP-NCAR reanalysis. However, in the Atlantic,

the response in the streamfunction in the UNCOUPLED integration is weak compared to either the COUPLED simulation or the NCEP-NCAR reanalysis.

d. Local air-sea relationship

A second explanation for the differences in the SAM precipitation variability between the COUPLED and UNCOUPLED runs can arise from differences in the local air-sea relationships. In this subsection the in situ precipitation and SST relationship over the Atlantic is examined. Following Wang et al. (2005) the precipitation and SST correlations are plotted for a one-month lead, zero lead/lag, and a one-month lag in Fig. 9. The climatological wind fields at 850 hPa for the UNCOUPLED and COUPLED integrations are also overlaid to identify the SACZ from the circulation, which is along the southwestern edge of the subtropical

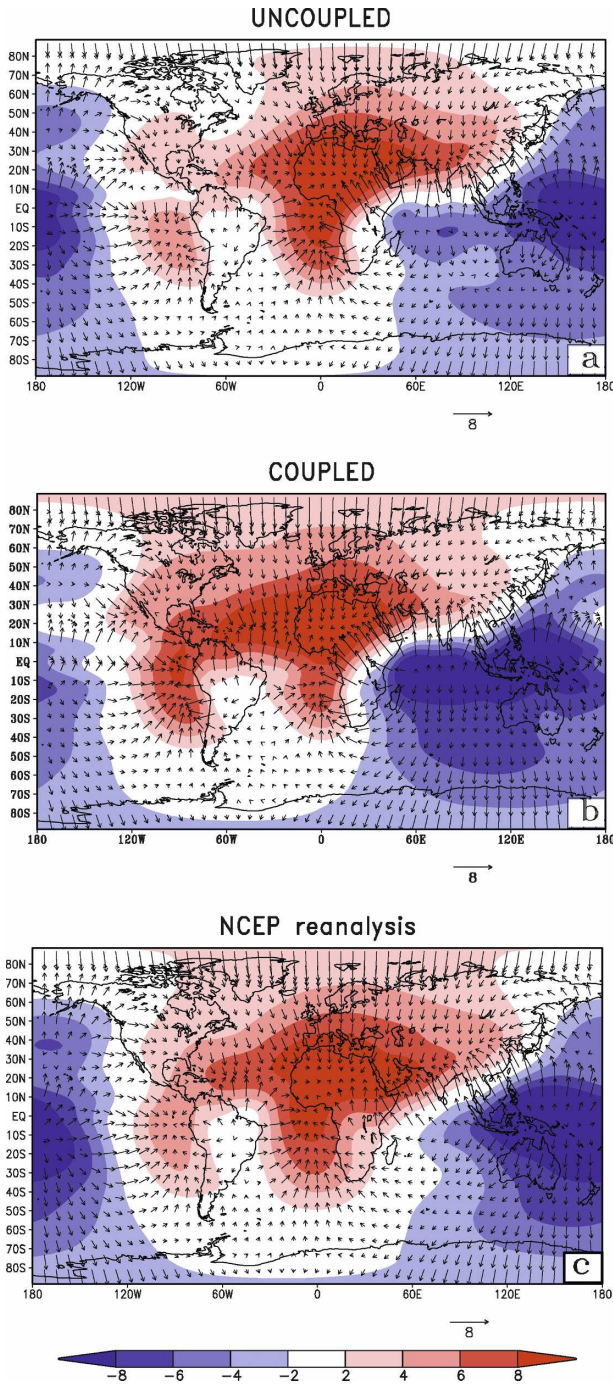


FIG. 6. Climatological mean DJF velocity potential and divergent wind at 200 hPa from (a) UNCOUPLED and (b) COUPLED integrations and (c) NCEP–NCAR reanalysis. Units: $1.0 \times 10^{-6} \text{ m}^2 \text{ s}^{-1}$.

high in the South Atlantic Ocean. In the observations (Figs. 9a–c) the SACZ region displays a negative (positive) correlation off the southeastern coast of Brazil (over the central and eastern south Atlantic Ocean) at

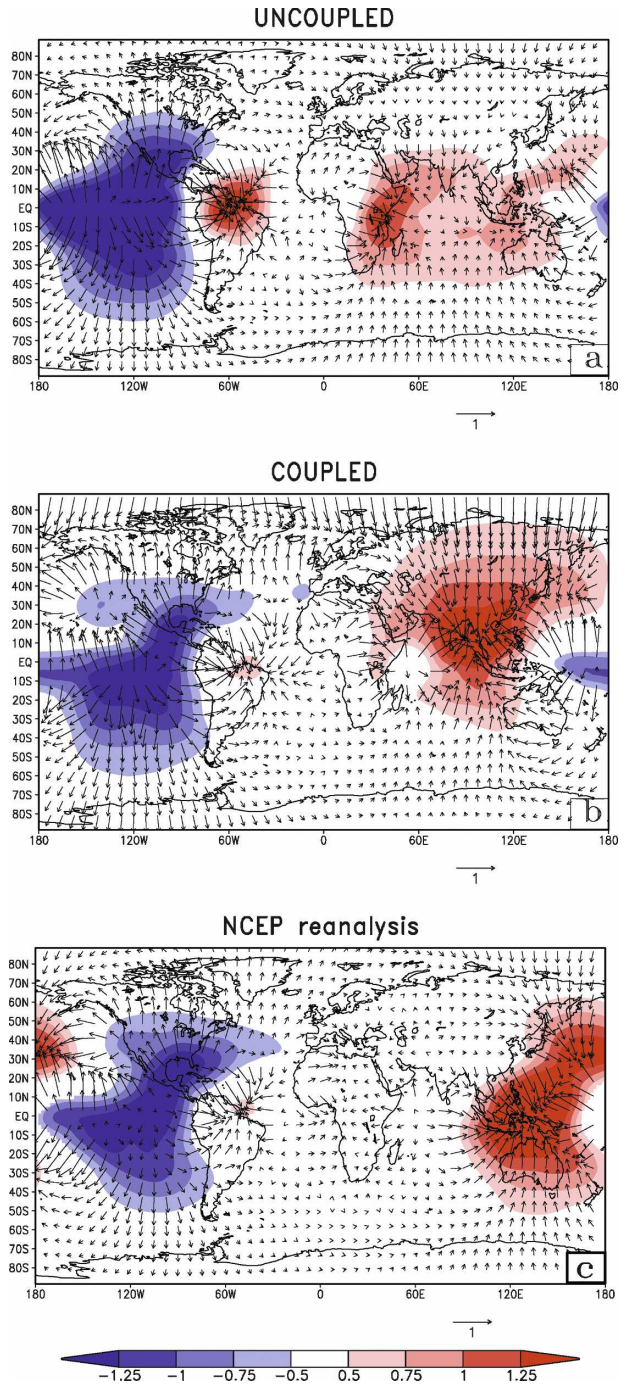


FIG. 7. Regression of the mean DJF velocity potential and divergent wind at 200 hPa on SST averaged over the Niño-3 region from (a) UNCOUPLED and (b) COUPLED integrations and (c) NCEP–NCAR reanalysis. In the case of UNCOUPLED integration the HADISST is used for computing the Niño-3 SST index. The unit of velocity potential (wind) is $1.0 \times 10^{-6} \text{ m}^2 \text{ s}^{-1}$ (m s^{-1}). Velocity potential significant at 10% significance according to a t test is plotted.

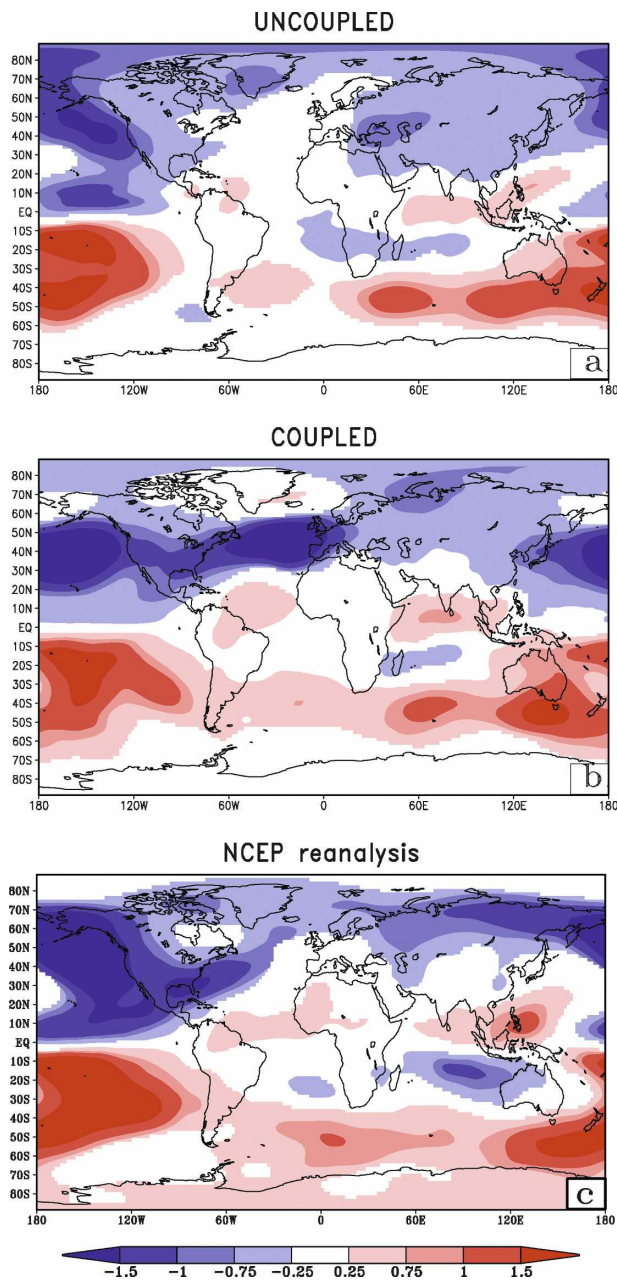


FIG. 8. Regression of the mean DJF streamfunction at 850 hPa on SST averaged over the Niño-3 region from (a) UNCOUPLED and (b) COUPLED integrations and (c) NCEP-NCAR reanalysis. In the case of UNCOUPLED integration the HADISST is used for computing the Niño-3 SST index. The units of velocity potential (winds) are in $1.0 \times 10^{-6} \text{ m}^2 \text{ s}^{-1}$. Only significant values at the 90% confidence interval according to a t test are shaded for the velocity potential.

all lead/lag times. Chaves and Nobre (2004) in their coupled modeling study showed that intensification of the SACZ results in cooling the underlying ocean surface through the reduction of the incident shortwave

solar radiation. They also showed that the Ekman pumping was about an order of magnitude less than the thermodynamic feedback between the SST and the shortwave radiative flux, suggesting that the atmosphere forces the upper ocean. In Figs. 9d–f the UNCOUPLED model contrary to the observations shows positive correlations over the SACZ region at all lead times, suggesting that the precipitation from the AGCM is forced by the underlying SST anomalies. In comparison, the COUPLED model shows a distinct negative correlation between the two variables over the SACZ region and south of 30°S at contemporaneous times (Fig. 9h) and when precipitation leads SST by one month (Fig. 9g). Qualitatively this compares well with the corresponding observations in Figs. 9b and 9a, respectively. However, the COUPLED run displays significant model bias such as the appearance of the relatively large positive correlations north of 20°S , which is most severe at zero lag (Fig. 9h) and when rain rate lags SST by one month (Fig. 9i).

As pointed out in Nobre et al. (2006) the SAM precipitation variability is intricately connected to the SACZ variability, and therefore these local precipitation–SST relationships over the region assume greater significance. Furthermore, both the large-scale atmospheric forcing and the local in situ forcing can potentially modulate the horizontal gradients of SST anomalies, which has implications on the surface winds (Lindzen and Nigam 1987; Misra 2007) and, therefore, on the precipitation variability through modulation of the surface convergence.

e. Land feedback

In addition to the role of the large-scale circulation and the local air–sea interactions, the land–atmosphere feedback also plays a critical role in the SAM variability (Xue et al. 2006, and references therein). To diagnose this feedback, the number of contiguous days by which evaporation is correlated in a statistically significant manner with the precipitation (with the former leading the latter) is shown in Fig. 10. Here we use the most recent version of the Global Offline Land Surface Dataset (GOLD) (Dirmeyer and Tan 2001) as our basis for observations. GOLD uses hybrid sets of meteorological forcing data that have been produced by combining the 40-yr ECMWF Re-Analysis (ERA-40) with the Global Precipitation Climatology Center (GPCC) (Rudolf et al. 1994) monthly precipitation estimates. One other attractive aspect of this validation dataset is that the same version of the SSiB land surface scheme is used to generate GOLD as used in the COUPLED and UNCOUPLED integrations. The GOLD dataset is available from 1960 to 2002.

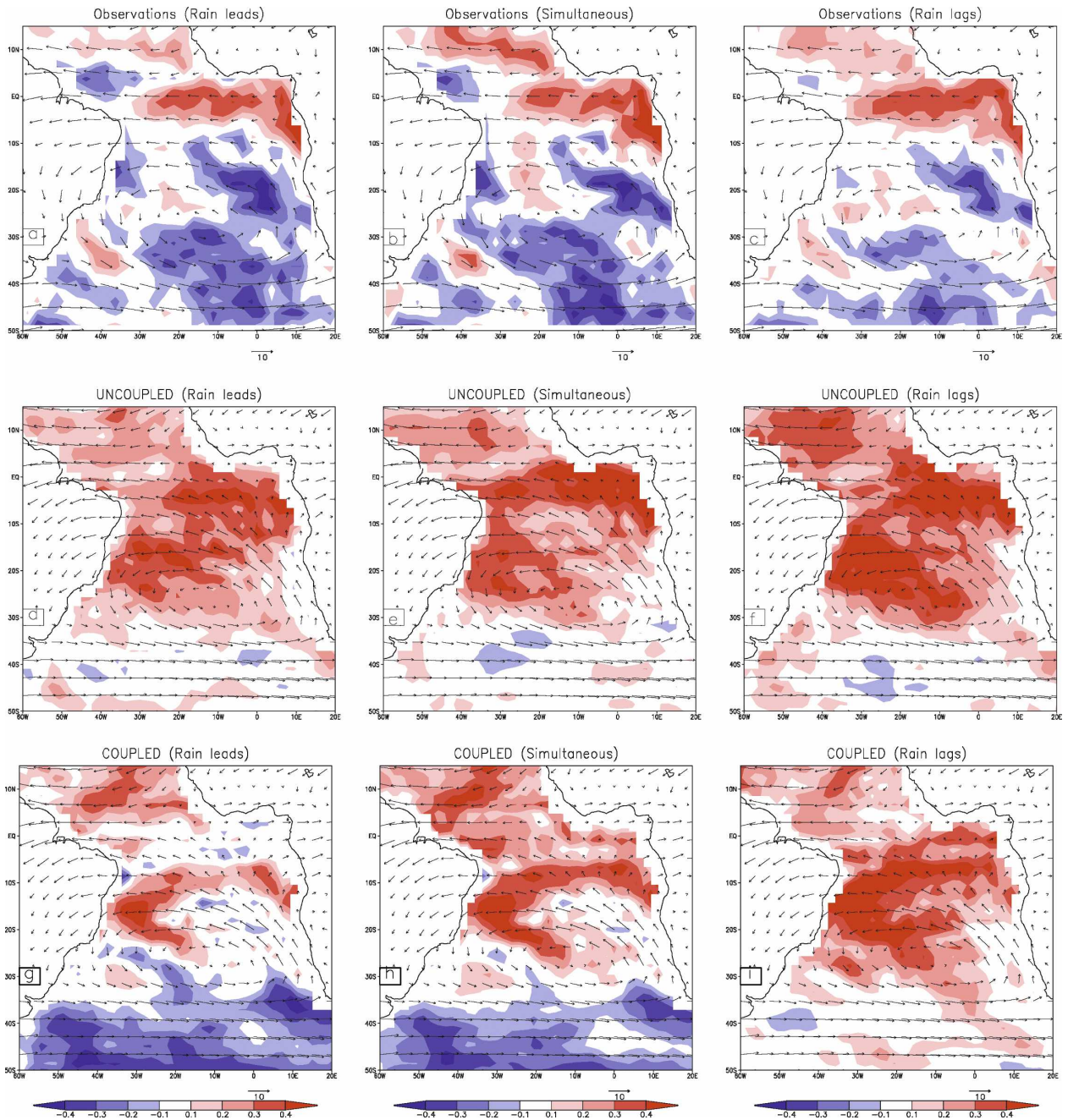


FIG. 9. Pointwise correlation between monthly mean precipitation and SST anomalies computed for DJF from observations with (a) precipitation leading SST by one month, (b) zero lead/lag, and (c) precipitation lagging SST by one month (overlaid with the climatological mean DJF 850-hPa wind field from NCEP–NCAR reanalysis). Similarly correlations from UNCOUPLED runs are shown (overlaid with the climatological DJF 850-hPa wind field) with (d) precipitation leading SST by one month, (e) zero lead/lag, and (f) precipitation lagging SST by one month. Corresponding correlations (overlaid with the corresponding climatological DJF 850-hPa wind field) from COUPLED integrations are shown with (g) precipitation leading SST by 1 month, (h) zero lead/lag, and (i) precipitation lagging SST by one month. Units of wind speed: m s^{-1} ; correlations are computed monthly and then averaged over the 3 months.

Clearly, the COUPLED model in Fig. 10b displays a longer lag/lead relationship between evaporation and precipitation, especially over the ARB and over the SAM region (albeit, with a COUPLED model bias of a

relatively shorter lag in the southeast corner of the SAM core), which brings it closer to the GOLD dataset shown in Fig. 10c. The UNCOUPLED integration (Fig. 10a), unlike the COUPLED run or the GOLD analysis,

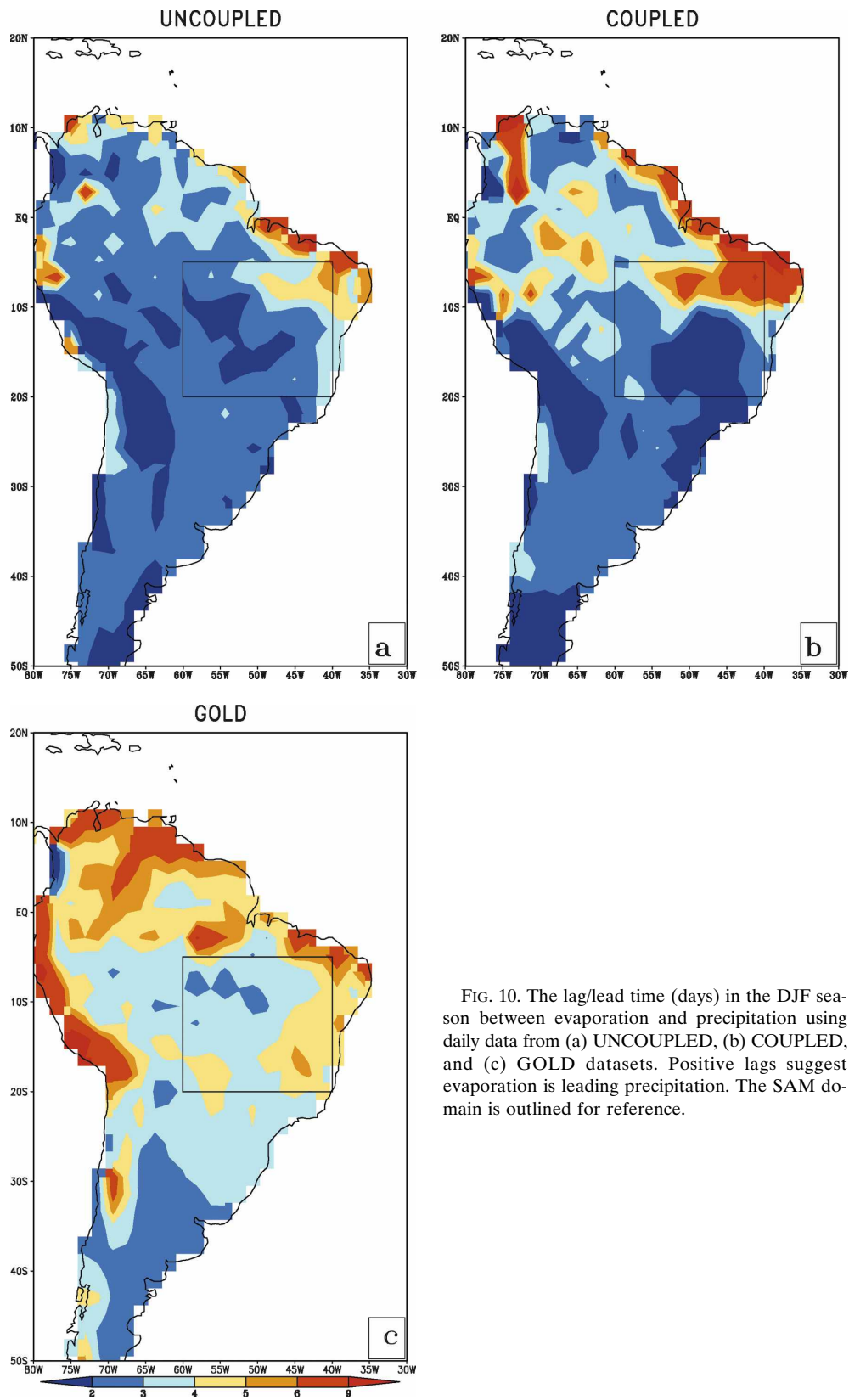


FIG. 10. The lag/lead time (days) in the DJF season between evaporation and precipitation using daily data from (a) UNCOUPLED, (b) COUPLED, and (c) GOLD datasets. Positive lags suggest evaporation is leading precipitation. The SAM domain is outlined for reference.

shows a much smaller lead time relationship of evaporation with precipitation. The area-averaged lead time of evaporation over precipitation in the SAM (ARB) domain in the UNCOUPLED run is 2.7 (2.6) days, in the COUPLED run is 3.1 (3.6) days, and in observations is 3.8 (4.1) days.

The autocorrelation time of the daily precipitation over continental South America in the DJF season (defined as the average of the time in days when the autocorrelation falls below significance level for 90 degrees of freedom based on t test) is shown in Fig. 11. The UNCOUPLED simulation in Fig. 11a has a much shorter decorrelation time over continental South America than either the COUPLED run (Fig. 11b) or the GOLD analysis. This is consistent with the previous figure (Figs. 10b and 10c): areas with increased lead time of the influence of evaporation on precipitation in the austral summer season over continental South America (Fig. 10) is coincident with areas of increased decorrelation time of precipitation (Fig. 11). In other words it implies that land–atmosphere feedback is prolonging the duration of the wet (or dry) events in the COUPLED simulation and GOLD analysis over the SAM and the ARB regions. It may be noted that the autocorrelation of the daily GOLD precipitation dataset validates rather nicely with independent rain gauge data over the eastern coast of Brazil (Misra 2008).

5. Discussion and conclusions

It is shown in this study that a coupled modeling framework is necessary to simulate the dominant interannual variation of the SAM precipitation associated with the ENSO variability. The conventional tier-2 approach of prescribing observed SST to force the COLA AGCM results in variability of SAM precipitation that is disconnected from the Niño-3 SST variation. A physical basis for the contrasting results between the two approaches stems from the major role of air–sea coupling in modulating the large-scale east–west divergent wind circulation, the in situ precipitation–SST variability over the SACZ region, and the land–atmosphere feedback over the ARB and the SAM regions.

In the coupled ocean–atmosphere COLA model (COUPLED experiment) the ascending cell of the climatological east–west Walker circulation is centered over the warm pool in the western Pacific Ocean, which extends westward over the equatorial Indian Ocean. In contrast, the uncoupled (to ocean) COLA atmospheric model (UNCOUPLED experiment) exhibits an ascending cell centered over the warm pool region in the western Pacific Ocean and extending eastward toward

the date line. The anomalous east–west circulation associated with the Niño-3 SST variability in the UNCOUPLED experiment displayed too strong a descent over the ARB region during a warm ENSO event. In contrast, the COUPLED experiment had a weaker descent over the ARB region similar to that depicted by the NCEP–NCAR reanalysis. In addition to this important difference in the large-scale upper-level circulation between the two modeling frameworks, the models also display important differences in the low-level circulation anomalies. The UNCOUPLED experiment exhibits very weak variability of the storm tracks in relation to the Niño-3 SST anomalies in the North Pacific and in the South Atlantic. In contrast, the COUPLED simulation, consistent with the NCEP–NCAR reanalysis, shows a significant linear relationship between storm track variability in the South Atlantic Ocean and Niño-3 SST anomalies.

The precipitation–SST relationship over the SACZ region, which also has a role in modulating the precipitation variability over the SAM region, shows important variations between the two modeling frameworks. In the COUPLED experiment, as in observations, there is a significant negative correlation of precipitation and SST over the subtropical South Atlantic Ocean when precipitation leads SST by one month and at zero lag. The UNCOUPLED experiment is unable to simulate this negative correlation. This suggests that the observed atmospheric forcing on SST variations over the SACZ region is best captured when air–sea coupling is considered in the modeling framework.

It is also shown that the surface evaporation over land in continental South America leads the precipitation variability by a few days in both an offline land data assimilation product and in the COUPLED simulation. This in turn further augments the decorrelation time of the daily precipitation over the region in the austral summer season, implying the prolongation of the wet (or dry) events. The UNCOUPLED simulation is found lacking in such a robust land–atmosphere feedback.

Another important feature as pointed in Misra (2008) is that air–sea coupling in the COUPLED run enhances the global tropical subseasonal variance, especially at the synoptic scales. This in turn enables propagating rain-bearing systems to move onshore and precipitate over land. The strong land–atmosphere interactions prevalent in the monsoon regions of the globe, including SAM, then prolong the memory of this precipitation as gauged by its decorrelation time.

An attempt of this study is to highlight that the conventional notion of defining potential seasonal predictability for the SAM region based on AGCM integra-

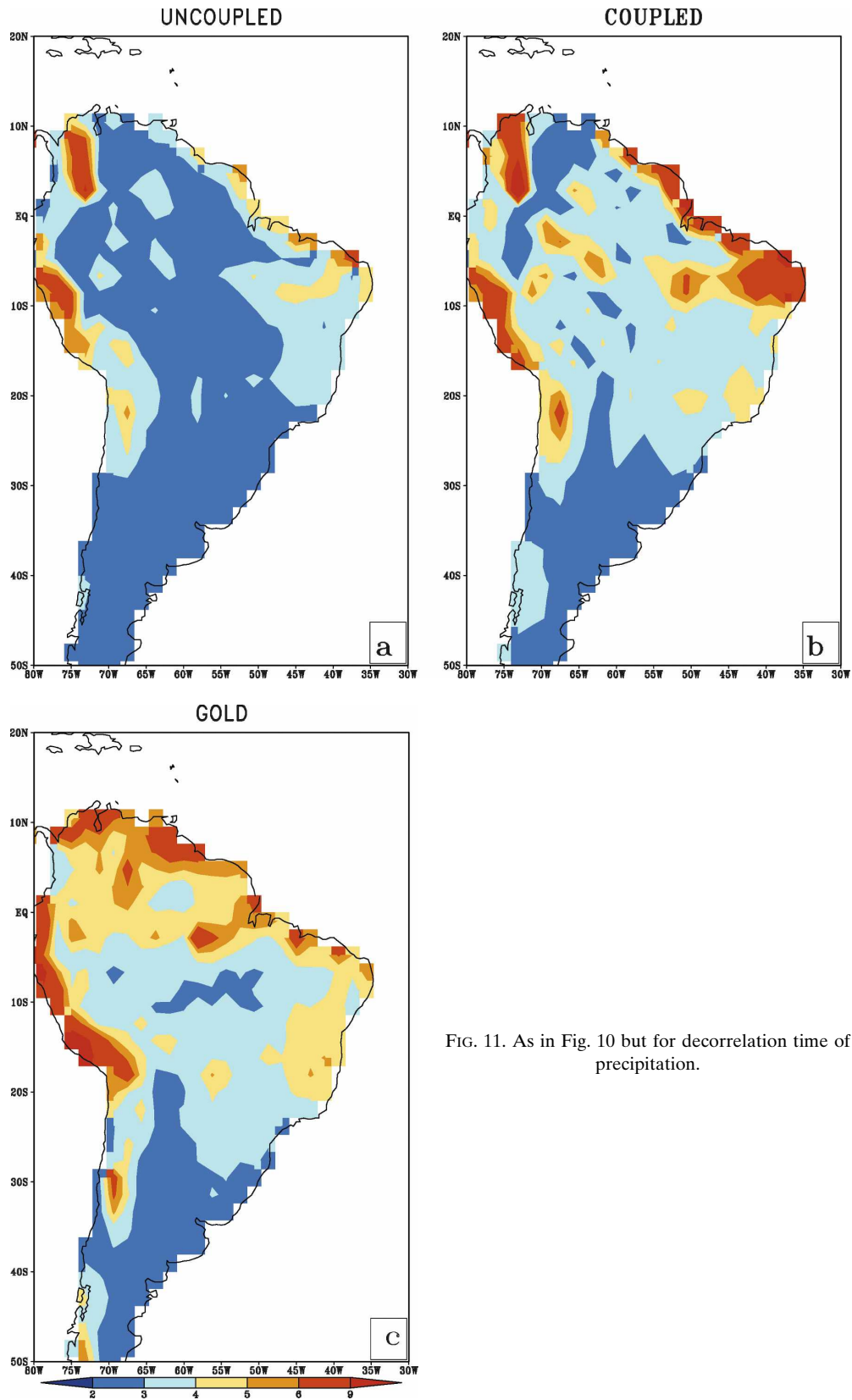


FIG. 11. As in Fig. 10 but for decorrelation time of precipitation.

tions forced with observed SST is inappropriate. Coupled air–sea interactions both in a local region (SACZ) and globally have important implications on SAM precipitation variability. This is to be tempered, however, with the fact that other neighboring regions in South America, such as the ARB, are not as sensitive to air–sea coupling in the modeling framework. Additionally, coupled predictions with current state-of-the-art coupled climate models are a challenge in itself. Misra et al. (2008) show that coupled model prediction made with realistic initial conditions of atmosphere and ocean yield results that may be quite different from long-term integrations from the same coupled model. These differences are attributed to initialization problems and model bias. Despite these issues coupled ocean–atmosphere modeling is providing new hope for improving the seasonal–interannual prediction of the monsoons.

Obviously the results presented here are not model independent. However, the physical basis for the differences in the coupled and uncoupled versions of the COLA AGCM is persuasive to conclude that air–sea coupling is important for the simulation of the SAM interannual precipitation variability.

Acknowledgments. This study was supported by NSF Grant ATM0332910, NASA Grant NNG04GG46G, and NOAA Grant NA04OAR4310034. The use of computing resources at the NASA Ames facility under NASA Project NNG06GB54G and Columbia Project SMD05-0115 is also acknowledged.

REFERENCES

- Bacmeister, J., P. J. Pegion, S. D. Schubert, and M. J. Suarez, 2000: *Atlas of Seasonal Means Simulated by the NSIPP-1 Atmospheric GCM*. Vol. 17, NASA Tech. Memo. 104606, 194 pp.
- Barnston, A. G., A. Kumar, L. Goddard, and M. P. Hoerling, 2005: Improving seasonal prediction practices through attribution of climate variability. *Bull. Amer. Meteor. Soc.*, **86**, 59–72.
- Bengtsson, L., U. Schlese, E. Roeckner, M. Latif, T. Barnett, and N. Graham, 1993: A two-tiered approach to long-range climate forecasting. *Science*, **261**, 1026–1029.
- Charney, J. G., and J. Shukla, 1981: Predictability of monsoons. *Monsoon Dynamics*, J. Lighthill, Ed., Cambridge University Press, 99–100.
- Chaves, R. R., and P. Nobre, 2004: Interactions between sea surface temperature over the South Atlantic Ocean and the South Atlantic Convergence Zone. *Geophys. Res. Lett.*, **31**, L03204, doi:10.1029/2003GL018647.
- Collins, W. D., and Coauthors, 2006: The Community Climate System Model Version 3 (CCSM3). *J. Climate*, **16**, 2122–2143.
- Dirmeyer, P. A., and F. J. Zeng, 1999: Precipitation infiltration in the Simplified SiB land surface scheme. *J. Meteor. Soc. Japan*, **77**, 291–303.
- , and L. Tan, 2001: A multi-decadal global land-surface data set of state variables and fluxes. COLA Tech. Rep. 102, 46 pp. [Available online at http://grads.iges.org/pubs/ctr_102.pdf.]
- Folland, C. K., A. W. Colman, D. P. Rowell, and M. K. Davey, 2001: Predictability of northeast Brazil rainfall and real-time forecast skill, 1987–98. *J. Climate*, **14**, 1937–1958.
- Gadgil, S., and S. Sajani, 1998: Monsoon precipitation in the AMIP runs. *Climate Dyn.*, **14**, 659–689.
- Garreaud, R. D., 2000: Cold air intrusions over subtropical South America: Mean structure and dynamics. *Mon. Wea. Rev.*, **128**, 2544–2559.
- , and J. M. Wallace, 1998: Summertime incursions of midlatitude air into subtropical and tropical South America. *Mon. Wea. Rev.*, **126**, 2713–2733.
- Gates, W. L., 1992: AMIP: The Atmospheric Model Intercomparison Project. *Bull. Amer. Soc.*, **73**, 1962–1970.
- , and Coauthors, 1999: An overview of the results of the Atmospheric Model Intercomparison Project (AMIP I). *Bull. Amer. Meteor. Soc.*, **80**, 29–55.
- Gent, P. R., and J. C. McWilliams, 1990: Isopycnal mixing in ocean circulation models. *J. Phys. Oceanogr.*, **20**, 150–155.
- Goddard, L., and S. Mason, 2002: Sensitivity of seasonal climate forecasts to persisted SST anomalies. *Climate Dyn.*, **19**, 619–632, doi:10.1007/s00382-002-0251-y.
- Grimm, A. M., 2004: How do La Niña events disturb the summer monsoon system in Brazil? *Climate Dyn.*, **22**, 123–138.
- , V. R. Barros, and M. E. Doyle, 2000: Climate variability in southern South America associated with El Niño and La Niña events. *J. Climate*, **13**, 35–58.
- , S. Ferraz, and J. Gomez, 2003: The El Niño impact on the summer monsoon in Brazil: Regional processes versus remote influences. *J. Climate*, **16**, 263–280.
- , C. S. Vera, and C. R. Mechoso, 2005: The South American monsoon system. *The Global Monsoon System: Research and Forecast Meteorology*, WMO TD-1266, 219–239.
- Hong, S. Y., and H. L. Pan, 1996: Nonlocal boundary layer vertical diffusion in a medium range forecast model. *Mon. Wea. Rev.*, **124**, 2322–2339.
- Kalnay, E., and Coauthors, 1996: The NCEP/NCAR 40-Year Reanalysis Project. *Bull. Amer. Meteor. Soc.*, **77**, 437–471.
- Kiehl, J. T., J. J. Hack, G. Bonan, B. A. Boville, D. L. Williamson, and P. J. Rasch, 1998: The National Center for Atmospheric Research Community Climate Model: CCM3. *J. Climate*, **11**, 1131–1149.
- Kinter, J. L., III, M. J. Fennessy, V. Krishnamurthy, and L. Marx, 2004: An evaluation of the apparent interdecadal shift in the tropical divergent circulation in the NCEP–NCAR reanalysis. *J. Climate*, **17**, 349–361.
- Kousky, V. E., 1985: Atmospheric circulation changes associated with rainfall anomalies over tropical Brazil. *Mon. Wea. Rev.*, **113**, 1951–1957.
- , 1988: Pentad outgoing longwave radiation climatology for the South American sector. *Rev. Bras. Meteor.*, **3**, 217–231.
- Kumar, K. K., M. Hoerling, and B. Rajagopalan, 2005: Advancing dynamical prediction of Indian monsoon rainfall. *Geophys. Res. Lett.*, **32**, L08704, doi:10.1029/2004GL021979.
- Large, W. G., J. C. McWilliams, and S. C. Doney, 1994: Oceanic vertical mixing: A review and a model with a nonlocal boundary layer parameterization. *Rev. Geophys.*, **32**, 363–403.
- Liebmann, B., G. N. Kiladis, J. A. Marengo, T. Ambrizzi, and J. D. Glick, 1999: Submonthly convective variability over South America and the South Atlantic convergence zone. *J. Climate*, **12**, 1877–1891.

- Lindzen, R. S., and S. Nigam, 1987: On the role of sea surface temperature gradients in forcing low-level winds and convergence in the tropics. *J. Atmos. Sci.*, **44**, 2418–2436.
- Marengo, J. A., B. Liebmann, V. Kousky, N. Filizola, and I. Wainer, 2001: On the onset and end of the rainy season in the Brazilian Amazon Basin. *J. Climate*, **14**, 833–852.
- Misra, V., 2004: An evaluation of the predictability of austral summer season precipitation over South America. *J. Climate*, **17**, 1161–1175.
- , 2006: Understanding the predictability of seasonal precipitation over northeast Brazil. *Tellus*, **58A**, 307–319.
- , 2007: A sensitivity study of the coupled simulation of the Northeast Brazil rainfall variability. *J. Geophys. Res.*, **112**, D11111, doi:10.1029/2006JD008093.
- , 2008: Coupled interactions of the monsoons. *Geophys. Res. Lett.*, **35**, L12705, doi:10.1029/2008GL033562.
- , and L. Marx, 2007: Manifestation of remote response over the equatorial Pacific in a climate model. *J. Geophys. Res.*, **112**, D20105, doi:10.1029/2007JD008597.
- , and —, 2008: The coupled seasonal hindcasts of the South American Monsoon. *Int. J. Climatol.*, in press.
- , and Coauthors, 2007: Validating and understanding ENSO simulation in two coupled climate models. *Tellus*, **59A**, 292–308.
- , L. Marx, M. Fennessy, B. Kirtman, and J. L. Kinter III, 2008: A comparison of climate prediction and simulation over tropical Pacific. *J. Climate*, **21**, 3601–3611.
- Moorthi, S., and M. Suarez, 1992: A parameterization of moist convection for general circulation models. *Mon. Wea. Rev.*, **120**, 978–1002.
- Newman, M., P. D. Sardeshmukh, and J. W. Bergman, 2000: Indian monsoon–ENSO relationship on interdecadal timescale. *J. Climate*, **13**, 579–595.
- Nobre, P., J. A. Marengo, I. F. A. Cavalcanti, and G. Obregon, 2006: Seasonal-to-decadal predictability and prediction of South American Climate. *J. Climate*, **19**, 5988–6004.
- Pacanowski, R. C., and S. M. Griffies, 1998: MOM3.0 manual. NOAA/Geophysical Fluid Dynamics Laboratory, 638 pp.
- Paegle, N.-J., and K. Mo, 2002: Linkages between summer rainfall variability over South America and sea surface temperature anomalies. *J. Climate*, **15**, 1389–1407.
- Rayner, N. A., D. E. Parker, E. B. Horton, C. K. Folland, L. V. Alexander, D. P. Rowell, E. C. Kent, and A. Kaplan, 2002: Global analyses of sea surface temperature, sea ice, and night marine air temperature since the late nineteenth century. *J. Geophys. Res.*, **108**, 4407, doi:10.1029/2002JD002670.
- Redi, M. H., 1982: Oceanic isopycnal mixing by coordinate rotation. *J. Phys. Oceanogr.*, **12**, 1154–1158.
- Reynolds, R. W., N. A. Rayner, T. M. Smith, D. C. Stokes, and W. Wang, 2002: An improved in situ and satellite SST analysis for climate. *J. Climate*, **15**, 1609–1625.
- Rudolf, B., H. Hauschild, W. Reuth, and U. Schneider, 1994: Terrestrial precipitation analysis: Operational method and required density of point measurements. *Global Precipitation and Climate Change*, M. Desbois and F. Desalmond, Eds., NATO ASI Series I, Vol. 26, Springer-Verlag, 173–186.
- Seluchi, M., and J. A. Marengo, 2000: Tropical-midlatitude exchange of air masses during summer and winter in South America: Climatic aspects and extreme events. *Int. J. Climatol.*, **20**, 1167–1190.
- Shukla, J., D. A. Paolino, D. M. Straus, D. DeWitt, M. Fennessy, J. L. Kinter, L. Marx, and R. Mo, 2000: Dynamical seasonal predictions with the COLA atmospheric model. *Quart. J. Roy. Meteor. Soc.*, **126**, 2265–2291.
- Smagorinsky, J., 1963: General circulation experiments with the primitive equations: I. The basic experiment. *Mon. Wea. Rev.*, **91**, 99–164.
- Sperber, K. R., and Coauthors, 2001: Dynamical seasonal predictability of the Asian summer monsoon. *Mon. Wea. Rev.*, **129**, 2226–2248.
- Tiedtke, M., 1984: The effect of penetrative cumulus convection on the large-scale flow in a general circulation model. *Beitr. Phys. Atmos.*, **57**, 216–239.
- Vera, C., and Coauthors, 2006: Toward a unified view of the American monsoon systems. *J. Climate*, **19**, 4977–5000.
- Wang, B., I. S. Kang, and J. Y. Lee, 2004: Ensemble simulations of the Asian–Australian monsoon variability by 11 AGCMs. *J. Climate*, **17**, 803–818.
- , Q. Ding, X. Fu, I.-S. Kang, K. Jin, J. Shukla, and F. Doblas-Reyes, 2005: Fundamental challenge in simulation and prediction of summer monsoon rainfall. *Geophys. Res. Lett.*, **32**, L15711, doi:10.1029/2005GL022734.
- Wu, R., B. P. Kirtman, and K. Pegion, 2006: Local air–sea relationship in observations and model simulations. *J. Climate*, **19**, 4914–4932.
- Xie, P., and P. Arkin, 1996: Analysis of global monthly precipitation using gauge observations, satellite estimates, and numerical model predictions. *J. Climate*, **9**, 840–858.
- Xue, Y., P. J. Sellers, J. L. Kinter III, and J. Shukla, 1991: A Simplified Biosphere Model for global climate studies. *J. Climate*, **4**, 345–364.
- , F. J. Zeng, and C. A. Schlosser, 1996: SSiB and its sensitivity to soil properties: A case study using HAPEX-Mobilhy data. *Global Planet. Change*, **13**, 183–194.
- , F. de Sales, W.-P. Li, C. R. Mechoso, C. A. Nobre, and H.-M. Juang, 2006: Role of land surface processes in South American monsoon development. *J. Climate*, **19**, 741–762.
- Zhou, J., and K.-M. Lau, 1998: Does a monsoon climate exist over South America? *J. Climate*, **11**, 1020–1040.